Scripta Materialia 273 (2026) 117114

Contents lists available at ScienceDirect

Scripta Materialia

journal homepage: www.journals.elsevier.com/scripta-materialia

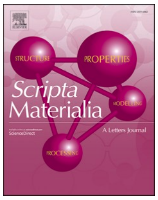

Thermal and athermal nucleation of MgSi co-clusters in Al-Mg-Si alloys

Ya Li [a,b,*], Robert Kahlenberg [a,c], Philipp Retzl [a,d], Ernst Kozeschnik [a]

[a] *Institute of Materials Science and Technology, TU Wien, Getreidemarkt 9, Vienna 1060, Austria*
[b] *State Key Laboratory of Powder Metallurgy, Central South University, Changsha 410083, China*
[c] *Materials Center Leoben Forschung GmbH, Roseggerstraße 12, Leoben 8700, Austria*
[d] *MatCalc Engineering GmbH, Gumpendorferstraße 21, 1060 Wien, Austria*

ARTICLE INFO

Keywords:
Al-Mg-Si alloy
Quenching
MgSi co-clusters
Thermal nucleation
Athermal nucleation

ABSTRACT

The interplay between thermal and athermal nucleation of MgSi co-clusters during quenching of solution-heat-treated Al-Mg-Si alloys is investigated through computer simulations. Thermal nucleation is typically described by classical nucleation theory, which refers to the formation of supercritical nuclei via the diffusion-controlled attachment of solute atoms to clusters of critical size. In the process of athermal nucleation, pre-existing subcritical nuclei become supercritical due to a decrease in critical size, for instance, as a result of increased undercooling during quenching. In this study, we develop a comprehensive nucleation model that integrates thermal and athermal contributions, offering new insights into the MgSi co-cluster formation in Al-Mg-Si alloys during continuous cooling. The results reveal that athermal nucleation is the predominant nucleation mechanism for MgSi co-clusters during quenching. Furthermore, the dependencies of thermal and athermal nucleation on cooling rate, temperature, and alloy composition are elucidated.

The process of nucleation marks the beginning of phase transformations. Classical Nucleation Theory (CNT), formulated in the early 20th century, is the most widely used theoretical model to quantitatively evaluate thermal nucleation kinetics. CNT builds upon the assumption that the subcritical atomic clusters exhibit a stationary “number density vs. size” distribution at a given chemical composition and temperature. The atomic clusters continuously change in size and composition as atoms attach to or detach from them. A nucleation event requires overcoming a defined energy barrier and exceeding the corresponding critical size by thermal and compositional fluctuations. This process is referred to as thermal activation or thermal nucleation. Although thermal nucleation can describe a wide range of nucleation events in nature [1,2], it is only strictly valid under conditions of constant temperature and a constant local chemical environment surrounding the nuclei.

In addition to the thermal nucleation (CNT) path, pre-existing subcritical embryos can also become supercritical when the critical size decreases as a result of, e.g., increasing chemical driving force under continuous cooling conditions. This process does not require thermal activation because the subcritical embryos are pre-existent and are “automatically” stabilized. This non-thermal activation of nuclei is referred to as athermal nucleation. It was first proposed by Fisher et al. [3] in 1948. Quested and Greer [4] then used it to describe athermal heterogeneous nucleation during solidification.

During quenching, solute cluster formation in Al-Mg-Si alloys exhibits characteristics of both thermal and athermal nucleation. However, models and simulations of cluster formation and precipitation in the Al-Mg-Si alloys have only considered the thermal nucleation path so far [2,3,5–9]. To account for the dual nature of the cluster nucleation mechanism, we propose a nucleation model that contains both the thermal and athermal characteristics that are present during continuous cooling. The model is applied to MgSi co-cluster nucleation in the Al-Mg-Si alloy system because of its imminent relevance to practical alloy engineering.

According to the quasi-equilibrium assumption of CNT, stationary subcritical clusters ($N(n,T), n < n^*$) maintain a Boltzmann distribution to minimize their total free energy [6], as illustrated in Fig. 1(a). n denotes the number of atoms in a cluster and n^* denotes the number of atoms in a critical cluster. Their equilibrium number density N at a given temperature T is given by [6]

$$N(n,T) = N_0 \exp\left(-\frac{\Delta G(n)}{k_B T}\right) \tag{1}$$

where N_0 is the number density of potential nucleation sites, $\Delta G(n)$ is the free energy change when forming a nucleus of size n, and k_B is the

---

* Corresponding author at: Institute of Materials Science and Technology, TU Wien, Getreidemarkt 9, Vienna 1060, Austria.
E-mail address: ya.li@tuwien.ac.at (Y. Li).

https://doi.org/10.1016/j.scriptamat.2025.117114
Received 7 July 2025; Received in revised form 9 October 2025; Accepted 21 November 2025

Boltzmann constant.

Fig. 1(a) shows the sketch of a stationary cluster size distribution $N(n, T)$ up to the critical size n^*, which is indicated by the vertical dashed line. N^* is the corresponding number density of equilibrium clusters of critical size n^*. The thermal and athermal nucleation mechanisms are indicated by right and left arrows, respectively. Thermal nucleation occurs when critical clusters exceed the critical size n^* through atomic attachment (black arrow in Fig. 1(a)). Athermal nucleation occurs when the pre-existing subcritical nuclei become stable as the decreasing critical size passes below their size, e.g., under continuous cooling conditions (red arrow in Fig. 1(a)).

When cooling from temperature T to a lower temperature $T - \Delta T$, the lagged actual cluster distribution $N(n, t)$ evolves toward to a new stationary cluster distribution $N(n, T - \Delta T)$, as shown in Fig. 1(b). This process occurs due to an increased driving force for cluster formation caused by increased undercooling. Nonetheless, the transition from $N(n, t)$ to $N(n, T - \Delta T)$ is not instantaneous but necessitates an incubation time τ (blue dashed arrow in Fig. 1(b)). The actual number density of critical clusters $N(n^*, t)$ (orange hollow spot B) is determined by the equilibrium one $N(n^*, T - \Delta T)$ (orange hollow spot A) and the current incubation time τ. It indicates the incubation time likewise affects both thermal and athermal transient nucleation, as indicated by the shadow areas in Fig. 1(b). The black and red shadow areas represent the contributions of thermal nucleation and athermal nucleation, respectively. Therefore, under continuous cooling conditions, both thermal and athermal nucleation are treated as non-stationary (transient) processes.

The stationary nucleation rate of clusters is a superposition of thermal (J_s^{th}) and athermal (J_s^{at}) components. It is expressed as

$$J_s = J_s^{th} + J_s^{at}. \tag{2}$$

When evaluating the stationary nucleation rate, it is assumed that the actual cluster distribution always corresponds to the stationary cluster distribution. Therefore, to a first approximation, the stationary nucleation rate can be formulated as

$$J_s = N(n^*, T)\cdot\beta^*\cdot Z + N(n^*, T)\cdot\dot{n}^*. \tag{3}$$

The first and second terms on the right-hand side correspond to the thermal (J_s^{th}) and athermal (J_s^{at}) stationary nucleation rates, respectively. $N(n^*, T)$ is the number density of equilibrium clusters with critical size n^* at temperature T, which equals $N_0 \exp(-\Delta G(n^*)/k_B T)$ with the number of potential nucleation sites N_0, and the energy barrier $\Delta G(n^*)$ for the formation of a critical nucleus. $\dot{n}^*$ is the change rate of the critical nucleus size n^*. β^* is the atomic attachment rate for critical nuclei [5]. For a multi-component system, it can be written as [5]

$$\beta^* = \frac{4\pi}{a^4}\cdot\frac{(r^*)^2}{V_m}\cdot\left[\sum_{i=1}^{\omega}\frac{(c_{ki}-c_{0i})^2}{c_{0i}D_{0i}}\right]^{-1}, \tag{4}$$

where r^* is the critical radius of the clusters, a is the interatomic distance, V_m is the molar volume of the matrix, c_{ki} and c_{0i} are the average concentrations of element i in precipitate k and the matrix, respectively. ω is the total number of elements, and D_{0i} is the effective tracer diffusion coefficient of element i in the matrix. Z is the Zeldovich factor [8]. For a spherical cluster, it can be expressed as [9]

$$Z = \left[-\frac{a^6}{64\pi^2}\cdot\frac{1}{k_B T}\cdot\frac{(\Delta G_V)^4}{(\gamma)^3}\right]^{1/2}. \tag{5}$$

where ΔG_V is the chemical driving force and γ is the size-dependent interfacial energy between the matrix and a cluster of critical size [10, 11].

The critical nucleus size n^* is expressed as

$$n^* = \frac{4}{3}\pi(r^*)^3\cdot\frac{1}{\Omega} \text{ with } r^* = \frac{2\gamma}{\Delta G_V}, \tag{6}$$

where Ω is the atomic volume.

The first derivative of the critical nucleus size n^* with respect to time t is

$$\dot{n}^* = \frac{4\pi}{3}\frac{1}{\Omega}\frac{d}{dt}(r^*)^3, \tag{7}$$

then the rate of the number of atoms in the critical cluster is obtained as

$$\dot{n}^* = \frac{-32\pi}{\Omega}\cdot\frac{\gamma^3}{(\Delta G_V)^4}\cdot\frac{\partial(dG_V)}{\partial T}\dot{T}. \tag{8}$$

As mentioned above, the equilibrium (stationary) distribution of clusters requires time to establish under continuous cooling conditions. Consequently, the actual nucleation rate $J(t)$ is related to the stationary nucleation rate J_s in a semi-phenomenological way. The commonly used expression is [7,12]

$$J(t) = J_s\cdot\exp\left(-\frac{\tau}{t}\right) = J_s^{th}\cdot\exp\left(-\frac{\tau}{t}\right) + J_s^{at}\cdot\exp\left(-\frac{\tau}{t}\right). \tag{9}$$

The first and second terms on the right-hand side correspond to the thermal (J^{th}) and athermal (J^{at}) non-stationary nucleation rates, respectively. Further illustrations of the stationary and non-stationary nucleation mechanisms are provided in the Supplementary file. The incubation time τ is largely determined by the diffusion coefficient of solutes and the chemical potential difference between the nucleus and the matrix. The expression proposed by Feder et al. [13] is used here as

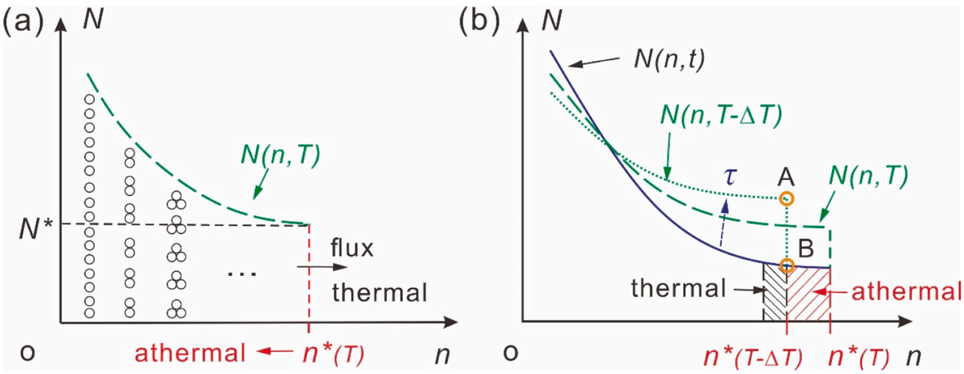

Fig. 1. Sketch of the possible nucleation mechanisms for atomic clusters. (a) Stationary thermal nucleation (black right arrow, atomic attachment-induced nucleation) and athermal nucleation (red left arrow, critical size reduction-induced nucleation). (b) Transient thermal and athermal nucleation when temperature T decreases to $T - \Delta T$. Within the incubation time τ, the actual cluster size distribution ($N(n, t)$, blue solid line) evolves towards the equilibrium cluster distribution at the reduced temperature ($N(n, T - \Delta T)$, green dotted line). Note that the y-axes in figure (a) and (b) are plotted on a logarithmic scale.

$$\tau = \frac{1}{2\beta^{*} Z^{2}}. \tag{10}$$

Practically, the incubation time τ is evaluated incrementally in each successive temperature interval during quenching, accounting for the fraction of the incubation time that has already passed in the simulation.

The thermal and athermal nucleation rates are calculated using Eq. (9). The present computational framework also considers the evolution of excess vacancy concentrations according to the vacancy annihilation kinetics model of Fischer et al. [14], and its impact on the acceleration of diffusional processes [15]. The interactions of vacancies with atomic solutes are also considered, as described in Refs. [16,17]. The Gibbs energy of the early MgSi co-clusters is described as a regular solution phase, as reported by Povoden-Karadeniz et al. [18]. The thermodynamics, diffusion kinetics, and interfacial energy (Generalized Broken-Bond model [9–11]) are automatically evaluated in the MatCalc software [19]. The average atomic volume of all elements in the aluminum alloy (Ω) is 1.661×10^{-29} m^3/atom. Other parameters, such as the interaction energy of solute atoms with vacancies, were reported by Peng et al. [20] and summarized by Li et al. [17].

Fig. 2(a) shows the nucleation energy when forming MgSi co-clusters of various sizes in a model Al-0.65Mg-0.6Si (wt. %) alloy. The alloy is cooled down from a typical solution annealing temperature of 540 °C to 25 °C. Before reaching the solvus temperature (approximately 210 °C), the co-cluster is thermodynamically unstable. The nucleation energy of clusters increases continuously with their size. Below the solvus temperature, the driving force becomes positive, and cluster formation becomes thermodynamically possible. At a typical paint-baking temperature of 185 °C used in automotive production, the critical cluster radius is approximately 4 nm. Below 100 °C, the nucleation barrier for critical cluster formation is significantly reduced, and the critical size falls into the sub-nanometer range. This will strongly promote cluster formation, in accordance with differential scanning calorimetry (DSC) and microstructural characterization data reported in the literature [21–26].

Fig. 2(b) shows the equilibrium cluster size distribution at different temperatures. At 540 °C, subcritical clusters contain only a few solute atoms, and their number density decreases rapidly with size (red solid line). This is expected because such clusters are thermodynamically unstable and exist only because of frequent compositional fluctuations. At 185 °C, the number density of subcritical clusters is still extremely low (blue wide dashed line). At 100 °C, the equilibrium cluster distribution shows a critical size of approximately 75 atoms (green dashed line), and the corresponding number density is approximately 10^7 m^{-3}. On further cooling from 100 °C to 25 °C, the number density of potential nuclei increases rapidly. At 25 °C, the clusters of critical size contain only about 15 atoms, and the corresponding equilibrium number density is approximately 10^{22} m^{-3}.

Fig. 3 shows the key parameters related to the co-cluster formation when cooling from 540 °C to 25 °C at different rates ranging from 1 K/s to 1000 K/s. One major observation is that the athermal nucleation rate is approximately 4–5 orders of magnitude larger than the corresponding thermal nucleation rate, as shown in Fig. 3(a) and (b). This indicates that the majority of clusters form during quenching through athermal nucleation rather than thermal nucleation. The calculated number density of clusters (thermal + athermal) decreases with increasing cooling rate (Fig. 3(c)), because the incubation time exponent $\exp(-\tau/t)$ remains much smaller under rapid cooling conditions (Fig. 4(d)). In addition, the temperature-dependent evolution of the atomic attachment rate β^{*} and the Zeldovich factor Z during cooling is shown in Fig. S2 of the Supplementary file, while the time-dependent evolution of the thermal and athermal nucleation rates is shown in Fig. S3.

At very fast cooling rates of 1000 K/s or higher, no co-clusters nucleation is observed (Fig. 3(c)). At intermediate cooling rates of 100–400 K/s, which are typical for water or liquid nitrogen quenching of Al alloys, approximately 10^2–10^{10} clusters per cubic meter form during cooling to 25 °C, with an average of ~15 atoms per cluster. The low cluster number density would not cause appreciable solute segregation, given the high number density of available Mg and Si atoms (~8×10^{26} m^{-3}). This aligns with the observations from the 3DAP measurements of the Al-0.4Mg-1Si (wt. %) alloy quenched with liquid nitrogen [27].

Fig. 4(a) shows the equilibrium cluster distributions at 90 °C for four Al-Mg-Si alloys with varying chemical compositions: Al-5Mg-5Si, Al-6Mg-6Si, Al-7Mg-7Si, and Al-8Mg-8Si (wt. %), which are denoted as 5Mg5Si, 6Mg6Si, 7Mg7Si, and 8Mg8Si, respectively. It shows that increasing the solute concentration rapidly decreases the critical size and increases the corresponding equilibrium number density of critical clusters (potential nuclei). When cooling the four alloys from 540 °C to 25 °C at 1 K/s, the nucleation rate increases rapidly with increasing solute content (Fig. 4(b)). Note that the nucleation rate depicted in Fig. 4 (b) is the sum of the thermal and athermal contributions, however, the athermal nucleation contribution is always dominant.

The higher solute concentration causes a higher driving force for cluster formation and a smaller critical nucleus size. This leads to the mean radius of the clusters in concentrated alloys being smaller at any given temperature (Fig. 4(c)). The incubation time exponential term is significantly larger in concentrated alloys (Fig. 4(d)). This is primarily due to the increased solute availability in concentrated alloys, which accelerates the attachment rate of solute atoms to subcritical clusters. Ultimately, the higher driving force, smaller critical radius, and shorter incubation time leads to a higher nucleation rate of the clusters.

Fig. 5 illustrates the variation of the athermal-to-thermal nucleation rate ratio (J^{at}/J^{th}) with cooling rate and alloy composition. For the Al-0.65Mg-0.6Si (wt. %) alloy, the athermal nucleation mechanism becomes increasingly dominant as the cooling rate increases (Fig. 5(a)). When alloys of different compositions are cooled from 540 °C to 25 °C at 1 K/s, the simulation shows that J^{at}/J^{th} decreases with increasing solute composition (Fig. 5(b)). Nevertheless, the athermal nucleation path remains dominant. Note that the rapid variations in J^{at}/J^{th} at high

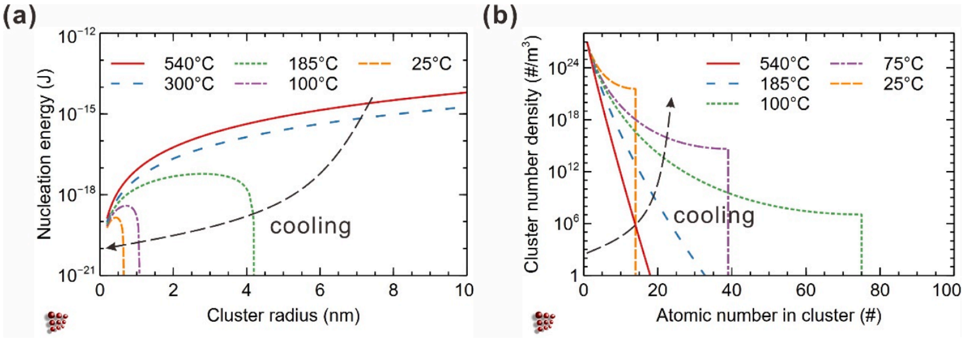

Fig. 2. Cooling of Al-0.65Mg-0.6Si (wt. %) alloy from a typical solution annealing temperature (540 °C) to room temperature (25 °C). (a) Nucleation energy of MgSi co-clusters of different sizes, and (b) calculated equilibrium distribution of MgSi co-clusters at different temperatures.

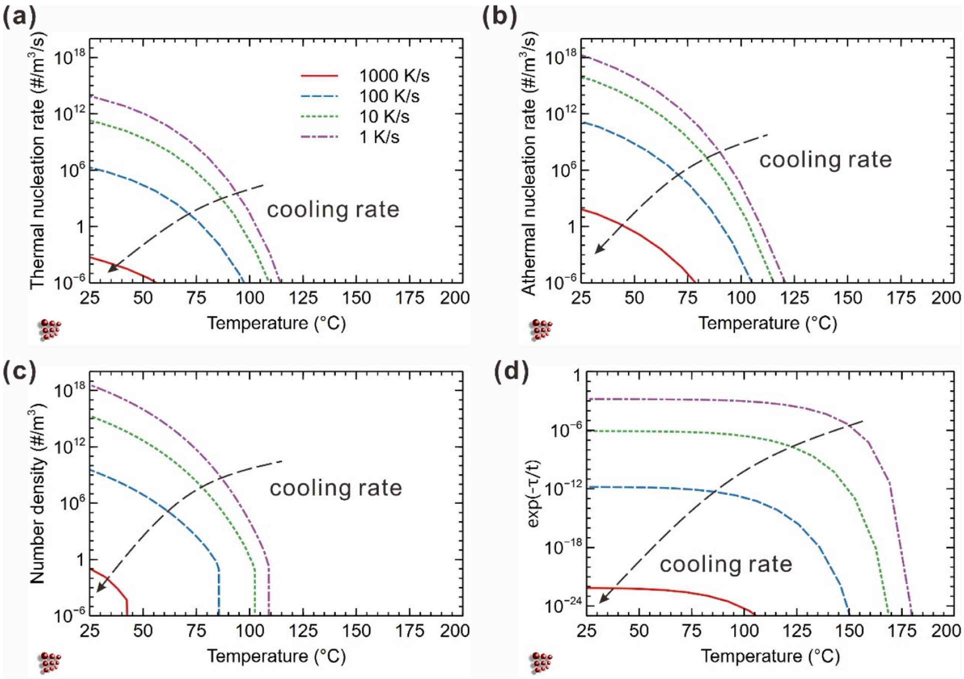

Fig. 3. The evolution of the (a) thermal nucleation rate, (b) athermal nucleation rate, (c) number density (thermal + athermal), and (d) incubation time exponential term of MgSi co-clusters while cooling the Al-0.65Mg-0.6Si (wt. %) alloy from 540 °C to 25 °C at different rates.

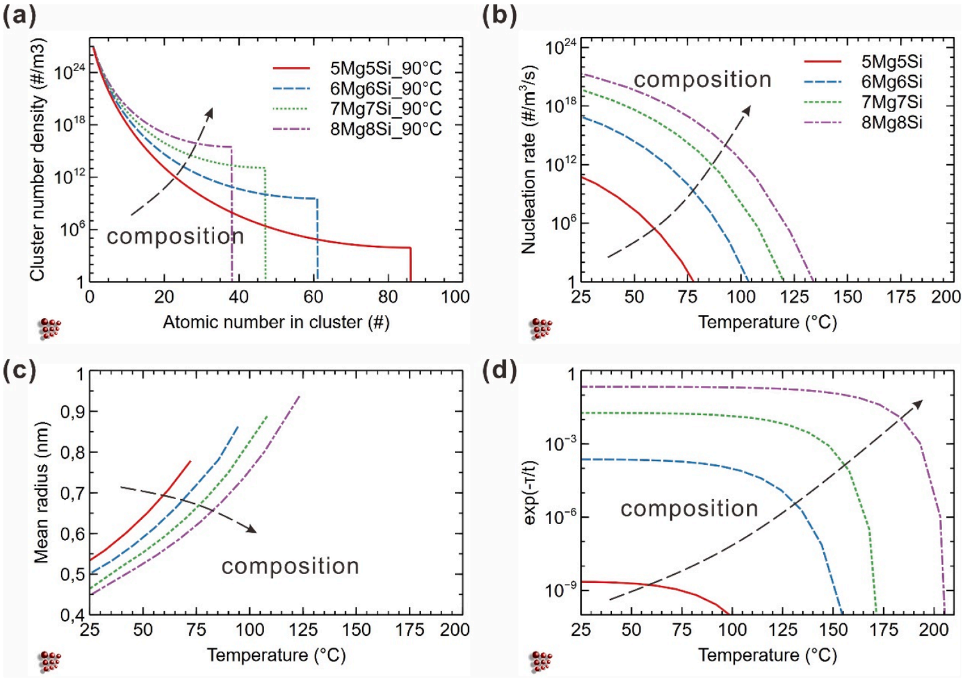

Fig. 4. Dependence of nucleation parameters on alloy concentration during cooling. (a) The equilibrium subcritical cluster distributions of four Al-Mg-Si (wt. %) alloys at 90 °C. When cooling the four alloys from 540 °C to 25 °C at 1 K/s: the evolution of the (b) nucleation rate, (c) mean radius, and (d) incubation time exponential term over temperature.

temperatures are of minor importance, given that the nucleation rates are extremely low in this regime.

The ratio of the athermal to thermal nucleation rates is calculated using Eqs. (3) and (9), which is

$$\frac{J^{at}}{J^{th}} = \frac{\dot{n}^*}{\beta^*\cdot Z}. \tag{11}$$

Inserting Eqs. (4), (5) and (8) delivers

$$\frac{J^{at}}{J^{th}} = C\cdot T^{1/2}\cdot\left[\sum_{i=1}^{n}\frac{(c_{ki}-c_{0i})^2}{c_{0i}D_{0i}}\right]\left[\frac{\partial(\Delta G_V)}{\partial T}\cdot\frac{1}{(\Delta G_V)^4}\right]\cdot\dot{T}, \tag{12}$$

which consists of five main terms. $C = 16\pi a N_A (k_B)^{1/2}\gamma^{5/2}$ can be considered as a roughly constant term, where N_A is the Avogadro constant. The second last term depends mainly on the chemical driving force

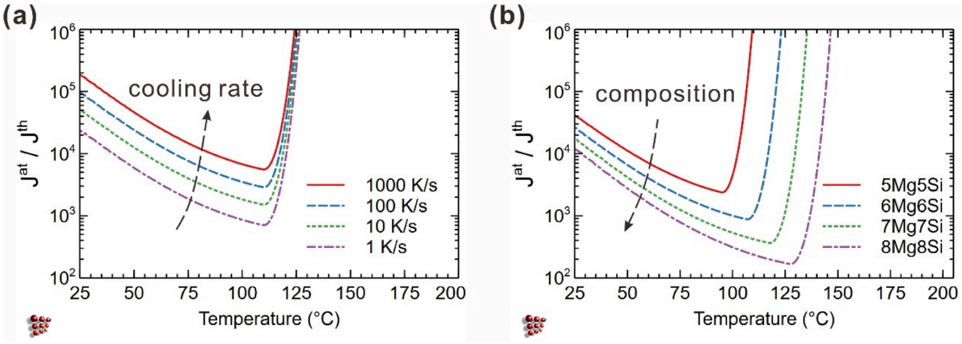

Fig. 5. Dependence of the ratio of athermal to thermal nucleation rates J^{at} / J^{th} on the (a) cooling rate and (b) alloy composition. (a) Cooling of the Al-0.65Mg-0.6Si (wt. %) alloy from 540 °C to 25 °C at different cooling rates. (b) Cooling of the four alloys from 540 °C to 25 °C at 1 K/s.

and it reflects the inverse correlation between the ratio J^{at} / J^{th} and the chemical driving force. This explains the decreasing dominance of athermal nucleation with increasing solute composition (Fig. 5(b)). The last term $\dot{T}$ indicates the increasing dominance of athermal nucleation with increasing cooling rates (Fig. 5(a)).

The ratio J^{at} / J^{th} increases as the temperature decreases, as shown in Fig. 5(a) and (b). This is because of the rapid exponential decline in the solute diffusion coefficient $D_{0i}(T)$ as the temperature T decreases. It also indicates that the athermal nucleation becomes increasingly dominant as solute diffusion diminishes.

In summary, the concept of "athermal nucleation" refers to a non-classical nucleation pathway where subcritical clusters evolve into supercritical ones as a result of the decreasing critical nucleus size, rather than through the attachment of monomers to critical clusters. A general model that integrates both thermal and athermal nucleation is developed. The model is used to investigate the MgSi co-cluster nucleation in Al-Mg-Si alloys under continuous cooling conditions. The simulations demonstrate that athermal nucleation is the dominant nucleation mechanism for MgSi co-clusters during quenching. And the dominance increases with increasing cooling rate, decreasing solute concentration, and decreasing solute diffusivity. Besides atomic cluster nucleation, the general nucleation model applies equally well to other nucleation events which were previously described only in terms of thermal nucleation.

CRediT authorship contribution statement

Ya Li: Writing – original draft, Methodology, Investigation, Conceptualization. **Robert Kahlenberg:** Writing – review & editing, Methodology. **Philipp Retzl:** Writing – review & editing, Methodology. **Ernst Kozeschnik:** Writing – review & editing, Supervision, Project administration, Methodology, Funding acquisition, Conceptualization.

Declaration of competing interest

The authors declare that they have no known competing financial interests or personal relationships that could have appeared to influence the work reported in this paper.

Acknowledgements

The authors acknowledge TU Wien Bibliothek for financial support through its Open Access Funding Programme.

Supplementary materials

Supplementary material associated with this article can be found, in the online version, at doi:10.1016/j.scriptamat.2025.117114.

References

[1] M. Sleutel, J. Lutsko, A.E.S. Van Driessche, M.A. Durán-Olivencia, D. Maes, Observing classical nucleation theory at work by monitoring phase transitions with molecular precision, Nat. Commun. 5 (2014) 1–8, https://doi.org/10.1038/NCOMMS6598.

[2] H. Vehkamäki, Classical nucleation theory in multicomponent systems, Class. Nucleation Theory Multicomponent Syst. (2006) 1–176, https://doi.org/10.1007/3-540-31218-8.

[3] J.C. Fisher, J.H. Hollomon, D. Turnbull, Nucleation, J. Appl. Phys. 19 (1948) 775–784, https://doi.org/10.1063/1.1698202.

[4] T.E. Quested, A.L. Greer, Athermal heterogeneous nucleation of solidification, Acta Mater. 53 (2005) 2683–2692, https://doi.org/10.1016/J.ACTAMAT.2005.02.028.

[5] J. Svoboda, F.D. Fischer, P. Fratzl, E. Kozeschnik, Modelling of kinetics in multi-component multi-phase systems with spherical precipitates: I: theory, Mater. Sci. Eng.: A 385 (2004) 166–174, https://doi.org/10.1016/J.MSEA.2004.06.018.

[6] D. Kashchiev, Nucleation: Basic Theory With Applications, Butterworth-Heinemann, 2000, https://doi.org/10.1016/B978-0-7506-4682-6.X5000-8.

[7] D. Turnbull, Transient nucleation, Met. Technol. 15 (4) (1948).

[8] K.C. Russell, Nucleation in solids: the induction and steady state effects, Adv. Colloid. Interface Sci. 13 (1980) 205–318, https://doi.org/10.1016/0001-8686(80)80003-0.

[9] E. Kozeschnik, Modeling Solid-State Precipitation, Momentum Press, LLC, 2012, https://doi.org/10.5643/9781606500644.

[10] B. Sonderegger, E. Kozeschnik, Size dependence of the interfacial energy in the generalized nearest-neighbor broken-bond approach, Scr. Mater. 60 (2009) 635–638, https://doi.org/10.1016/J.SCRIPTAMAT.2008.12.025.

[11] B. Sonderegger, E. Kozeschnik, Generalized nearest-neighbor broken-bond analysis of randomly oriented coherent interfaces in multicomponent fcc and bcc structures, Met. Mater. Trans. Phys. Met. Mater. Sci. 40 (2009) 499–510, https://doi.org/10.1007/S11661-008-9752-6.

[12] D. Kashchiev, Nucleation at variable supersaturation, Surf. Sci. 18 (1969) 293–297, https://doi.org/10.1016/0039-6028(69)90172-1.

[13] J. Feder, K.C. Russell, J. Lothe, G.M. Pound, Homogeneous nucleation and growth of droplets in vapours, Adv. Phys. 15 (1966) 111–178, https://doi.org/10.1080/00018736600101264.

[14] F.D. Fischer, J. Svoboda, F. Appel, E. Kozeschnik, Modeling of excess vacancy annihilation at different types of sinks, Acta Mater. 59 (2011) 3463–3472, https://doi.org/10.1016/J.ACTAMAT.2011.02.020.

[15] J.D. Robson, Deformation enhanced diffusion in aluminium alloys, Met. Mater. Trans. Phys. Met. Mater. Sci. 51 (2020) 5401–5413, https://doi.org/10.1007/S11661-020-05960-5.

[16] J. Svoboda, F.D. Fischer, Modelling for hydrogen diffusion in metals with traps revisited, Acta Mater. 60 (2012) 1211–1220, https://doi.org/10.1016/J.ACTAMAT.2011.11.025.

[17] Y. Li, R. Kahlenberg, P. Retzl, Y. Shan, Y. Du, E. Kozeschnik, Impact of atomic couples and pairs on quenched-In vacancies in Al-Mg-Si-Cu alloys, Scr. Mater. 271 (2026) 116970, https://doi.org/10.1016/j.scriptamat.2025.116970.

[18] E. Povoden-Karadeniz, P. Lang, P. Warczok, A. Falahati, W. Jun, E. Kozeschnik, CALPHAD modeling of metastable phases in the Al–Mg–Si system, Calphad 43 (2013) 94–104, https://doi.org/10.1016/J.CALPHAD.2013.03.004.

[19] E. Kozeschnik, Matcalc 6 - The Materials Calculator, (2017). https://www.matcalc.at (accessed May 28, 2025).

[20] J. Peng, S. Bahl, A. Shyam, J.A. Haynes, D. Shin, Solute-vacancy clustering in aluminum, Acta Mater. 196 (2020) 747–758, https://doi.org/10.1016/J.ACTAMAT.2020.06.062.

[21] M. Takeda, F. Ohkubo, T. Shirai, K. Fukui, Stability of metastable phases and microstructures in the ageing process of Al-Mg-Si ternary alloys, J. Mater. Sci. 33 (1998) 2385–2390, https://doi.org/10.1023/A:1004355824857/METRICS.

[22] I. Dutta, S.M. Allen, A calorimetric study of precipitation in commercial aluminium alloy 6061, J. Mater. Sci. Lett. 10 (1991) 323–326, https://doi.org/10.1007/BF00719697/METRICS.

[23] Z. Yang, J. Banhart, Natural and artificial ageing in aluminium alloys – the role of excess vacancies, Acta Mater. 215 (2021) 117014, https://doi.org/10.1016/J.ACTAMAT.2021.117014.

[24] A. Serizawa, H. Shoichi, T. Sato, 3DAP Characterization and thermal stability of nano-scale clusters in Al-Mg-Si alloys, Mater. Sci. Forum 519–521 (2006) 245–250, https://doi.org/10.4028/WWW.SCIENTIFIC.NET/MSF.519-521.245.

[25] A. Serizawa, S. Hirosawa, T. Sato, Three-dimensional atom probe characterization of nanoclusters responsible for multistep aging behavior of an Al-Mg-Si alloy, Met. Mater Trans. Phys. Met. Mater Sci. 39 (2008) 243–251, https://doi.org/10.1007/S11661-007-9438-5.

[26] C.S.T. Chang, J. Banhart, Low-temperature differential scanning calorimetry of an Al-Mg-Si alloy, Met. Mater Trans. Phys. Met. Mater Sci. 42 (2011) 1960–1964, https://doi.org/10.1007/s11661-010-0596-5.

[27] P. Dumitraschkewitz, S.S.A. Gerstl, P.J. Uggowitzer, J.F. Löffler, S. Pogatscher, Atom probe tomography study of As-quenched Al–Mg–Si alloys, Adv. Eng. Mater. 19 (2017), https://doi.org/10.1002/adem.201600668.